Power System Enterprise Control with Inertial Response Procurement

Aramazd Muzhikyan, *Student Member, IEEE,* Toufic Mezher, and Amro M. Farid, *Senior Member, IEEE*

***Abstract*—As the power system evolves to better address environmental and reliability concerns, its overall dynamics changes and consequently challenges the adequacy of established operating procedures. This evolution brings a significant increase in the number of integrated renewable energy sources (RES) and HVDC connections. RES are normally connected to the grid through power electronic converters, which reduces or completely eliminates their electrical coupling to the power grid. As a result, such units are unable to contribute to the inertia of the system, posing a potential threat to the grid's physical security. More specifically, post-fault frequency characteristics, such as rate of change of frequency (RoCoF), frequency nadir and quasi-steady-state frequency, depend on the system inertia and their respective limits may potentially be violated. One way to address this problem is adding constraints to the unit commitment formulation so that operations maintain their frequency characteristics within acceptable limits. This paper studies how such changes affect the system frequency deviation from its rated value. The power system is modeled as an enterprise control that combines multiple layers of control operations into one package. Such integration allows capturing how the effects of wind integration and the addition of unit commitment inertia constraints propagate through control layers to impact the system frequency.**

***Index Terms*—Power system enterprise control, power system inertia, power system dynamics**

NOMENCLATURE

f_0	system rated frequency
ω_0	system rated angular frequency
M	angular momentum at the rated frequency
D	damping parameter
$1/R$	net gain of the governor
K	automatic generation control (AGC) gain
T_{CH}	prime mover time constant (charging time)
T_G	governor time constant
J_i	moment of inertia of generator i
E_i	kinetic energy of generator i
E_{sys}	kinetic energy of the whole system
H_i	inertia constant of generator i
H_{sys}	inertia constant of the whole system
$\Delta f(t)$	system frequency deviation
$\Delta P_m(t)$	system mechanical power deviation
$\Delta P_e(t)$	system electrical power deviation
$\Delta P_V(t)$	valve position deviation
$\Delta P_{ref}(t)$	reference power
$\hat{P}^{DA}$	day-ahead demand forecast
$\hat{P}^{ST}$	short-term demand forecast
$\Delta\hat{P}^{ST}$	short-term demand increment forecast
P^{LF}	load following reserve requirement
R^{RP}	ramping reserve requirement
P^{RG}	regulation reserve requirement
$P(t)$	real-time actual demand
$\Delta P^{DA}(t)$	power imbalances at the SCUC output
$\Delta R^{DA}(t)$	ramping imbalances at the SCUC output
$\Delta P^{ST}(t)$	power imbalances at the SCED output
$\Delta P^{RT}(t)$	power imbalances in the real-time
$I(t), I_t$	residual system imbalances
C_i^U	shutdown cost of generator i
C_i^D	startup cost of generator i
C_i^F	fixed cost of generator i
C_i^L	linear cost of generator i
C_i^Q	quadratic cost of generator i
P_i^{max}	maximum power output of generator i
P_{sys}^{max}	maximum power output of the whole system
P_i^{min}	minimum power output of generator i
R_i^{max}	maximum ramping rate of generator i
F_l^{max}	maximum flow limit of line l
P_{it}	power output of generator i
ΔP_{it}	power increment of generator i
G_t	amount of regulation in use
F_{lt}	power flow level of line l
w_{it}	ON/OFF state of the generator i
w_{it}^u	startup indicator of the generator i
w_{it}^d	shutdown indicator of the generator i
N_B	number of buses
N_G	number of generators
B_{ji}	correspondence matrix of generator i to bus j
γ_{jt}	incremental transmission loss factor (ITLF) of bus j
a_{ljt}	bus j generation shift distribution factor (GSDF) to line l
T_h	scheduling time step (normally, 1 hour)
T_m	real-time market time step (normally, 5 minutes)

Manuscript received December 25, 2016.

A. Muzhikyan is with Thayer School of Engineering, Dartmouth College, 14 Engineering Drive, Hanover, NH 03755, USA. aramazd.muzhikyan.th@Dartmouth.edu

T. Mezher is with Faculty of Department of Industrial and Systems Engineering, Khalifa University, PO Box 54224, Abu Dhabi, UAE. tmezher@masdar.ac.ae

A. M. Farid is with Faculty of Thayer School of Engineering, Dartmouth College, 14 Engineering Drive, Hanover, NH 03755, USA. amfarid@dartmouth.edu; and a research affiliate at Massachusetts Institute of Technology, 77 Massachusetts Avenue Cambridge, MA, 02139, USA. amfarid@mit.edu

I. INTRODUCTION

As the power system evolves to better address environmental and reliability concerns, its overall dynamics changes and

consequently challenges the adequacy of established operating procedures [1]. This evolution brings a significant increase in the number of integrated renewable energy sources (RES) and HVDC connections. The variable nature of the RES creates additional challenges for the power system balancing operations and leads to increased requirements for operating reserves [2]–[4].

Besides the variability, the RES and the traditional generation units have differences from the perspective of system inertia. RES are normally connected to the grid through power electronic converters, which reduces or completely eliminates their electrical coupling to the power grid. As a result, such units are unable to contribute to the inertia of the system, posing a potential threat to the grid's physical security. Also, increasing penetration of RES into the power grid drives installation of more HVDC connections to accommodate the transmission of remotely generated renewable energy to the consumers. However, HVDC connections electrically decouple the parts of the system they connect, which results in a system with electrically decoupled areas with smaller inertia. Reduced system inertia alters the post-fault frequency dynamics and can have a negative impact on the frequency stability of the power grid [5].

Many studies have addressed this issue by integrating post-fault frequency requirements into different levels of power system operations, such as economic dispatch and unit commitment. A multi-period unit commitment problem with integrated primary frequency regulation constraints is proposed in [6]. The primary frequency regulation provision from each generation unit is modeled as a linear function of system frequency deviation, which refers to the steady-state value of the post-fault frequency deviation. In [7], [8], frequency control constraints are incorporated into the market dispatch model. Rate of change of frequency (RoCoF) and minimum frequency constraints are derived in terms of dispatch decision variables, which ensures that the generation dispatch meets the frequency control requirements. The authors of [9] have developed a set of constraints for the dispatch model to ensure adequate primary frequency response. These constraints are expressed as functions of the system inertia and governor response ramp rates. However, the load damping is ignored and the system inertia is assumed to be a known constant. A two-stage stochastic economic dispatch model with added frequency constraints is developed in [10]. Simplified dynamic models are used to derive the post-fault maximum frequency deviation constraints. In [11], a mixed-integer linear programming formulation for the stochastic unit commitment is proposed. A set of frequency constraints are introduced to ensure the post-fault frequency dynamics meets the RoCoF, frequency nadir and quasi-steady-state frequency requirements. Reference [12] derives a modified system frequency response model which is used to find an analytical representation of the system frequency nadir. The derived analytical expressions are later linearized by a piecewise linearization technique and integrated into the unit commitment problem. In contrast, the authors of [13] study how fast-response battery units can be used to maintain the frequency nadir and RoCoF within the desired limits. The outputs of battery units are adjusted immediately after loss of a generation to minimize the system imbalances. This control technique is integrated into the linearized unit commitment problem.

This paper studies how incorporating RoCoF and frequency nadir requirements into the unit commitment affects the system frequency variations in the real-time. This paper achieves this by making the following two contributions. First, expressions for inertial response requirements are derived that keep the system within the given RoCoF and frequency nadir limits. While such expressions have been derived in the literature before, the existing methods mainly use simplified models for generation control, usually consisting of the rotating mass and the frequency damping only. This reduces the system dynamics to a first order differential equation and significantly simplifies the derivations. However, this leaves out other major components of the generation control, such as the governor and the prime mover. This paper develops more generalized derivations that take the governor with primary control into account. The system dynamics is described by a second order differential equation in this case. The dynamics introduced by the prime mover are omitted in this paper to avoid over-complication of the derivations and will be addressed in the future work. Next, after the expressions for inertial response requirements are derived, the second step is to study how these requirements, that are designed to constrain certain aspects of frequency variations, affect the real-time frequency profile. To this end, the inertial response requirements are incorporated into the unit commitment problem. This gives an insight into how the presence of these constraints changes the commitment of the generation units for different scenarios of the RES integration. However, in order to obtain the real-time frequency profile, the dynamics of the physical power grid should be modeled and simulated for the generators scheduled by the unit commitment. Additionally, the dynamic model should receive generation setpoints from the real-time market, that dispatches the generation units to new levels every 5-15 minutes. Thus, to achieve the goal of this paper, different layers of the power system operations should be modeled and simulated together.

As shown in Fig. 1, the power system operations are modeled as a multi-layer hierarchical control on top of the physical power grid called *enterprise control* [1]. It has been used to systematically study the integration of renewable energy [14], [15], energy storage [16], and demand side resources [17]. The primary advantage of enterprise control is that it demonstrates how changes in one control layer will propagate through the other control layers to impact the grid's physical behavior. For the purposes of this study, two modifications are made to the enterprise control simulator. First, new constraints are added to the unit commitment problem that ensure the RoCoF and the frequency nadir are always within the acceptable limits during the system operations. Second, the steady-state model of the physical power grid and the regulation service are replaced with their corresponding dynamic models. This gives access to the notion of system frequency otherwise absent in the steady-state model.

The paper is organized as follows. Section II presents the background information on the power system generation control and inertia. Section III derives the RoCoF and the

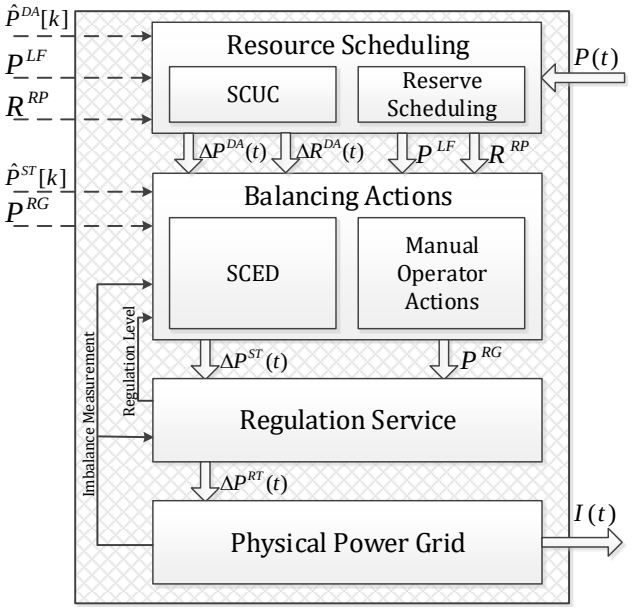

Fig. 1. Power system enterprise control simulator model [14], [15]

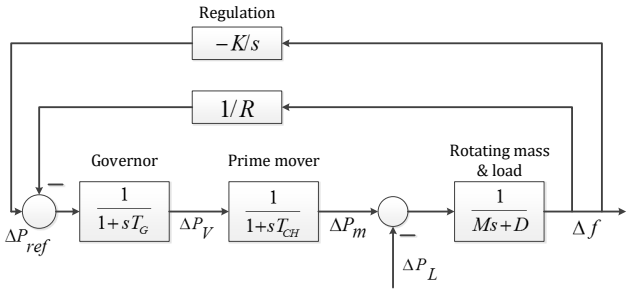

Fig. 2. Power system generation control [18], [19]

frequency nadir as functions of the generator's dynamic characteristics. Section IV briefly describes the enterprise control simulator used for this study and the introduced modifications to facilitate the needs of this study. Section V describes the system configurations and the simulation scenarios used in this paper. Section VI discusses the results and Section VII presents the conclusions.

II. Background

This section provides background information on the power system generation control and inertia.

A. Power System Generation Control

The general form of the generation dynamic control block diagram is presented in Fig. 2 [18], [19]. It consists of four main components, namely rotating mass & load, prime mover, governor and regulation. The mathematical formulation of each block is described in this subsection.

First, the rotating mass & load block is described by the following first order equation [18]:

$$M\frac{\mathrm{d}\Delta f(t)}{\mathrm{dt}} + D\cdot\Delta f(t) = \Delta P_m(t) - \Delta P_e(t) \tag{1}$$

where M is the angular momentum of the machine at the rated frequency. D is the damping parameter that indicates the sensitivity of the frequency-dependent load on the system frequency. $\Delta P_m(t)$ and $\Delta P_e(t)$ are the changes of the mechanical and electrical powers of the system respectively.

The prime mover, be it a steam or hydro turbine, drives the generator. The simplest nonreheat turbine is described by a first order equation and relates the mechanical power output ΔP_m to the position of the valve ΔP_V [18]:

$$T_{CH}\frac{\mathrm{d}\Delta P_m(t)}{\mathrm{dt}} + \Delta P_m(t) = \Delta P_V(t) \tag{2}$$

where T_{CH} is a time constant called charging time.

The governor controls the input valve to maintain the system frequency at the rated value. The simplest governor is described by a first order equation and relates the valve position ΔP_V to the system frequency deviation $\Delta f(t)$ [18]:

$$T_G\frac{\mathrm{d}\Delta P_V(t)}{\mathrm{dt}} + \Delta P_V(t) = \Delta P_{ref}(t) - \frac{1}{R}\Delta f(t) \tag{3}$$

where $1/R$ is the net gain of the governor and T_G is a time constant. $1/R$ feedback loop is also called primary control. However, the governor is unable to wholly restore the system frequency after a change of the load ΔP_L occurs.

The regulation service, implemented as an automatic generation control (AGC), restores the frequency to the rated value by measuring the system frequency deviation Δf and adjusting the reference power ΔP_{ref} [19]:

$$\Delta P_{ref}(t) = -K\cdot\int\Delta f(t)\mathrm{dt} \tag{4}$$

Regulation service is also called secondary control.

B. Inertia from Synchronous Generation

The power system inertia is the resistance of the synchronous generators and turbines to the rotational speed change. The kinetic energy of the generator i rotating at ω_0 rated angular frequency can be written as [5]:

$$E_i = \frac{J_i\omega_0^2}{2} \tag{5}$$

where J_i is the moment of inertia of the generator i. It is important to mention the relation between the angular momentum M and the kinetic energy E:

$$E = \frac{f_0\cdot M}{2} \tag{6}$$

The kinetic energy in (5) is often normalized to the maximum power output P_i^{max} and is called the inertia constant H_i [5]. Inertia constant defines the duration the generator is able to provide maximum power only using the stored kinetic energy (5):

$$H_i = \frac{E_i}{P_i^{max}} \tag{7}$$

Since the system frequency is the same for all throughout the network, all generators can be combined into one. Thus, the total energy stored in the system is:

$$E_{sys} = \sum_{i=1}^{N} E_i = \sum_{i=1}^{N} H_i\cdot P_i^{max} \tag{8}$$

Thus, the combined inertia constant of all synchronous generators can be written as [5]:

$$H_{sys} = \frac{E_{sys}}{P_{sys}^{max}} = \frac{\sum_{i=1}^{N} H_i \cdot P_i^{max}}{\sum_{i=1}^{N} P_i^{max}} \tag{9}$$

III. Rate of Change of Frequency (RoCoF) and Frequency Nadir Determination

Rate of change of frequency (RoCoF) and frequency nadir are two important characteristics of the port-fault system frequency dynamics [5]. The RoCoF is the initial rate at which the frequency changes immediately after a contingency happens and is critical to reliable power system operation. Frequency nadir, on the other hand, is the minimum level the frequency drops following the event, before recovering to its steady-state value. If the RoCoF or the frequency nadir exceed their allowed limits, the generator protection may trigger disconnecting it from the grid.

A. Frequency Deviation Profile

Expressions for the RoCoF and the frequency nadir can be derived from the frequency deviation profile $\Delta f(t)$, the solution of the power system dynamic equations (1)-(4). As stated above, this paper ignores the dynamics introduced by the prime mover, $\Delta P_V(t) = \Delta P_m(t)$. Also, the calculations of these frequency characteristics are carried out in the absence of the regulation service, $\Delta P_{ref}(t) = 0$. Thus, the system boils down to the following couple of differential equations:

$$M\frac{\mathrm{d}\Delta f(t)}{\mathrm{dt}} + D\cdot\Delta f(t) = \Delta P_m(t) - \Delta P_e(t) \tag{10}$$

$$T_G\frac{\mathrm{d}\Delta P_m(t)}{\mathrm{dt}} + \Delta P_m(t) = -\frac{1}{R}\Delta f(t) \tag{11}$$

For the rest of the calculations the subscript in T_G will be skipped for simplicity of equations, i.e., $T \equiv T_G$ assignment is used. Also, $\Delta P_e(t)$ is assumed to be a step function with a magnitude ΔP. Thus, (10) and (11) can be combined into the following second order differential equation:

$$MT\frac{\mathrm{d}^2\Delta f(t)}{\mathrm{dt}^2} + (DT+M)\frac{\mathrm{d}\Delta f(t)}{\mathrm{dt}} + \left(D+\frac{1}{R}\right)\Delta f(t) = -\Delta P \tag{12}$$

The roots of the characteristic equation for (12) are:

$$x = \frac{-(DT+M) \pm \sqrt{(DT-M)^2 - \dfrac{4MT}{R}}}{2MT} \tag{13}$$

Thus, the solution of (12) can be represented as:

$$\Delta f(t) = C_1 e^{x_1 t} + C_2 e^{x_2 t} \tag{14}$$

where x_1 and x_2 are the roots of the characteristic equation (13), and C_1 and C_2 are constants defined by the initial conditions of (12). Thus, when both x_1 and x_2 are real numbers, according to (14), the system frequency decreases exponentially towards the quasi-steady-state value, without having a frequency nadir. This goes against the purpose of this paper to study the impact of the system inertia on frequency nadir and RoCoF. In contrast, when x_1 and x_2 are both complex numbers, the solution (14) becomes a *sine* profile with exponentially decreasing magnitude. This guarantees presence of frequency nadir, which is at the core of this paper's interest. Thus, in order for x_1 and x_2 to be complex, the expression under the square root in (13) should be negative:

$$(DT-M)^2 < \frac{4MT}{R} \tag{15}$$

When the assumption (15) holds, the solution of (12) can be written as:

$$\Delta f(t) = \left(-\frac{1}{D+1/R} + \left(A\cos\beta t + B\sin\beta t\right)e^{-\alpha t}\right)\Delta P \tag{16}$$

where α and β are real and imaginary parts of (13) respectively:

$$\alpha = \frac{DT+M}{2MT}, \qquad \beta = \frac{\sqrt{\dfrac{4MT}{R} - (DT-M)^2}}{2MT} \tag{17}$$

To calculate A and B, the following initial conditions are taken into account. First, the frequency deviation is still small immediately after the loss of a generation unit, $\Delta f(0) \approx 0$. As a result, the governor response is also negligible, $\Delta P_m(0) \approx 0$ [11]. These initial conditions yield A and B as:

$$A = \frac{1}{D+1/R}, \qquad B = \frac{1}{\beta}\left(\frac{\alpha}{D+1/R} - \frac{1}{M}\right) \tag{18}$$

Equations (16)-(18) are used in the following subsections to derive the RoCoF and the frequency nadir.

B. Rate of Change of Frequency (RoCoF)

Once the frequency deviation profile in (16)-(18) is obtained, the next step is to calculate the derivative of the frequency deviation in (16):

$$\frac{\mathrm{d}\Delta f(t)}{\mathrm{dt}} = \Big((B\beta - A\alpha)\cos\beta t - (B\alpha + A\beta)\sin\beta t\Big)e^{-\alpha t}\Delta P \tag{19}$$

Thus, using (17) and (18), the RoCoF is calculated from (19):

$$RoCoF = \frac{\mathrm{d}\Delta f(0)}{\mathrm{dt}} = (B\beta - A\alpha)\Delta P = -\frac{\Delta P}{M} \tag{20}$$

Using (6) and (8), RoCoF takes the following final form:

$$RoCoF = -\frac{f_0\cdot\Delta P}{2E_{sys}} = -\frac{f_0\cdot P_k^{max}}{2\cdot\sum_{\substack{i=1\\ i\neq k}}^{N} H_i\cdot P_i^{max}} \tag{21}$$

C. Frequency Nadir

First, the time t_n when the system reaches its nadir is determined. Since the frequency derivative should be zero at nadir, t_n is determined by equating the right-hand-side of (19) to zero. Thus, using (17) and (18):

$$\tan\beta t_n = \frac{B\beta - A\alpha}{B\alpha + A\beta} = \frac{\dfrac{\alpha}{D+1/R} - \dfrac{1}{M} - \dfrac{\alpha}{D+1/R}}{\dfrac{1}{\beta}\left(\dfrac{\alpha^2+\beta^2}{D+1/R} - \dfrac{\alpha}{M}\right)} \tag{22}$$

The expression $\alpha^2+\beta^2$ is calculated separately using (17):

$$\alpha^2+\beta^2=\frac{(DT+M)^2+4MT/R-(DT-M)^2}{4M^2T^2}=\frac{D+1/R}{MT} \tag{23}$$

Substituting (23) into (22), we get:

$$\tan\beta t_n=\frac{2MT\beta}{DT-M} \tag{24}$$

The arctangent function is used to extract t_n from (24). However, since the range of the arctangent output is $[-\pi/2;\pi/2]$, t_n can have a negative value when $DT-M<0$. To avoid this, the range is shifted to $[0;\pi]$ by adding π to the arctangent output when $DT-M<0$:

$$t_n=\begin{cases}\dfrac{1}{\beta}\arctan\left(\dfrac{2MT\beta}{DT-M}\right), & \text{if } DT-M\geq 0\\ \dfrac{1}{\beta}\left(\arctan\left(\dfrac{2MT\beta}{DT-M}\right)+\pi\right), & \text{if } DT-M<0\end{cases} \tag{25}$$

Now, once t_n is obtained, it can be substituted into (16) to calculate the frequency nadir. The calculations for different signs of $DT-M$ are slightly different, but yield the same results. Therefore, in the following derivations $DT-M>0$ is assumed. First, the trigonometric part of (16) is calculated:

$$\begin{aligned}&A\cos\beta t_n+B\sin\beta t_n=\cos\beta t_n\,(A+B\cdot\tan\beta t_n)=\\&=\frac{A+B\cdot\tan\beta t_n}{\sqrt{1+\tan^2\beta t_n}}=\frac{\dfrac{1}{D+1/R}+\left(\dfrac{\alpha}{D+1/R}-\dfrac{1}{M}\right)\cdot\dfrac{2MT}{DT-M}}{\sqrt{1+4M^2T^2\beta^2/(DT-M)^2}}=\\&=\frac{\dfrac{DT-M}{D+1/R}+\left(\dfrac{DT+M}{2MT(D+1/R)}-\dfrac{1}{M}\right)\cdot 2MT}{\sqrt{(DT-M)^2+4M^2T^2\beta^2}}=\\&=\frac{\dfrac{DT-M}{D+1/R}+\left(\dfrac{DT+M-2T(D+1/R)}{2MT(D+1/R)}\right)\cdot 2MT}{\sqrt{(DT-M)^2+4MT/R-(DT-M)^2}}=\\&=\frac{DT-M+DT+M-2T(D+1/R)}{(D+1/R)\sqrt{4MT/R}}=-\frac{\sqrt{RT/M}}{DR+1}\end{aligned} \tag{26}$$

Substituting (26) into (16) gives the frequency nadir:

$$\Delta f_{nadir}=-\frac{R+\sqrt{RT/M}}{DR+1}e^{-\alpha t_n}\Delta P \tag{27}$$

where t_n is given by (25). Thus, if Δf_{max} is the maximum of the frequency nadir absolute value, the following condition should hold:

$$\frac{R+\sqrt{RT/M}}{DR+1}e^{-\alpha t_n}P_k^{max}\leq\Delta f_{max} \tag{28}$$

However, the left-hand-side of (28) is a nonlinear function of M and cannot be directly integrated into the unit commitment problem as a constraint.

On the other hand, it can be shown that αt_n is a monotonically increasing function of M while condition (15) holds. As a result, the left-hand-side of (28) is a monotonically decreasing function of M. Thus, if M_k^* is the solution of:

$$\frac{R+\sqrt{RT/M}}{DR+1}e^{-\alpha t_n}P_k^{max}=\Delta f_{max} \tag{29}$$

the condition (28) holds as long as $M_k\geq M_k^*$ or, using (6):

$$\sum_{\substack{i=1\\ i\neq k}}^{N}H_i\cdot P_i^{max}\geq\frac{f_0M_k^*}{2} \tag{30}$$

It is important to notice that in (29), t_n depends on M too. As a result, it has no analytical solution and M_k^* is found by numerical solution.

IV. Power System Enterprise Control with Inertia Procurement

As mentioned in the introduction and depicted in Fig. 1, the power system operation is modeled as a multi-layer hierarchical control on top of the physical power grid. The control layers are resource scheduling, balancing operations and regulation service and the interested reader is referred to [14], [15] for a detailed description.

The original enterprise control formulation is modified to facilitate the needs of this study and are summarize as follows. First, new constraints are added to the unit commitment formulation that make sure the RoCoF and the frequency nadir limits are respected. Next, the original steady-state formulation of the physical power grid and the regulation service are replaced with a dynamic model described by the differential equations presented in Section II-A. Utilization of the dynamic model is necessary to introduce the concept of the system frequency into the simulations. A brief description of each control layer is presented in the following subsections.

A. Resource Scheduling

The resource scheduling layer is implemented as a security-constrained unit commitment problem (SCUC). The goal of the SCUC problem is to choose the right set of generation units, that are able to meet the real-time demand with minimum cost. In the original formulation, the SCUC problem is a nonlinear optimization problem with integrated power flow equations and system security requirements [20]. However, the constraints are often linearized to avoid convergence issues. The SCUC formulation in [14], [15] is amended here to include inertia constraints that keep the RoCoF and the frequency nadir within allowed limits:

$$\min\quad\sum_{t=1}^{24}\sum_{i=1}^{N_G}\left(w_{it}C_i^F+C_i^LP_{it}+C_i^QP_{it}^2+w_{it}^uC_i^U+w_{it}^dC_i^D\right) \tag{31}$$

$$\text{s.t.}\quad\sum_{i=1}^{N_G}P_{it}=\hat{P}_t^{DA} \tag{32}$$

$$-R_i^{max}T_h\leq P_{it}-P_{i,t-1}\leq R_i^{max}T_h \tag{33}$$

$$w_{it}P_i^{min}\leq P_{it}\leq w_{it}P_i^{max} \tag{34}$$

$$w_{it}=w_{i,t-1}+w_{it}^u-w_{it}^d \tag{35}$$

$$\sum_{\substack{k=1\\k\neq i}}^{N_G} w_{kt} H_k P_k^{max} \geq \frac{f_0 \cdot w_{it} P_i^{max}}{2 \cdot RoCoF^{max}} \tag{36}$$

$$\sum_{\substack{k=1\\k\neq i}}^{N_G} w_{kt} H_k P_k^{max} \geq \frac{f_0 \cdot w_{it} M_i^*}{2} \tag{37}$$

$$\sum_{i=1}^{N_G} w_{it} P_i^{max} - \sum_{i=1}^{N_G} P_{it} \geq P^{LF} \tag{38}$$

$$\sum_{i=1}^{N_G} P_{it} - \sum_{i=1}^{N_G} w_{it} P_i^{min} \geq P^{LF} \tag{39}$$

$$\sum_{i=1}^{N_G} w_{it} R_i^{max} - \sum_{i=1}^{N_G} \left(\frac{P_{it} - P_{i,t-1}}{T_h} \right) \geq R^{RP} \tag{40}$$

$$\sum_{i=1}^{N_G} \left(\frac{P_{it} - P_{i,t-1}}{T_h} \right) - \sum_{i=1}^{N_G} w_{it} R_i^{min} \geq R^{RP} \tag{41}$$

where i and t are generator and time indices respectively. The inertia constraints (36) and (37) are derived from (21) and (30) respectively, and include $\{w_{it}\}$ binary variables on both sides to allow generators to be switched on and off.

B. Balancing Actions

The real-time market moves available generator outputs to new setpoints (re-dispatch) in the most cost-efficient way. In its original formulation, generation re-dispatch is implemented as a non-linear optimization model, called AC optimal power flow (ACOPF) [21]. Due to problems with convergence and computational complexity [20], most of the U.S. independent system operators (ISO) moved from ACOPF to linear optimization models. The most commonly used model is called security-constrained economic dispatch (SCED) and is formulated as an incremental linear optimization problem [22]:

$$\min \quad \sum_{i=1}^{N_G} (C_i^L \Delta P_{it} + 2 C_i^Q P_{it} \Delta P_{it}) \tag{42}$$

$$\text{s.t.} \quad \sum_{j=1}^{N_B} (1 - \gamma_{jt}) \left(\sum_{i=1}^{N_G} B_{ji} \Delta P_{it} - \Delta \hat{P}_{jt}^{ST} \right) = I_t + G_t \tag{43}$$

$$\sum_{j=1}^{N_B} a_{ljt} \left(\sum_{i=1}^{N_G} B_{ji} \Delta P_{it} - \Delta \hat{P}_{jt}^{ST} \right) \leq F_l^{max} - F_{lt} \tag{44}$$

$$-R_i^{max} T_m \leq \Delta P_{it} \leq R_i^{max} T_m \tag{45}$$

$$P_{it} - P_i^{min} \leq \Delta P_{it} \leq P_i^{max} - P_{it} \tag{46}$$

where i, j, l and t are generator, bus, line and time indices respectively. Use of incremental values for generation and load allows incorporation of sensitivity factors and problem linearization. Sensitivity factors establish linear connections between changes of power injections on the buses and state-related parameters of the system [18]. Two sensitivity factors are used in the SCED. The incremental transmission loss factor (ITLF) for bus i shows how much the total system losses change, when power injection on bus i increases by a unit [23].

C. Regulation Service and Generation Control

The enterprise control simulator described in [14], [15] uses steady-state models for the regulation service and the physical power grid. In contrast, this paper uses generation control and regulation dynamic models described in Section II-A to study the impact of wind integration on the system frequency deviation. As mentioned above, for the simplicity of the model, this paper ignores the dynamics introduced by the prime mover, $\Delta P_V(t) = \Delta P_m(t)$, which yields to the following system of three linear differential equations:

$$M \frac{\mathrm{d}\Delta f(t)}{\mathrm{dt}} + D \cdot \Delta f(t) = \Delta P_m(t) - \Delta P_e(t) \tag{47}$$

$$T_G \frac{\mathrm{d}\Delta P_m(t)}{\mathrm{dt}} + \Delta P_m(t) = \Delta P_{ref}(t) - \frac{1}{R} \Delta f(t) \tag{48}$$

$$\frac{\mathrm{d}\Delta P_{ref}(t)}{\mathrm{dt}} = -K \cdot \Delta f(t) \tag{49}$$

where $\Delta P_e(t)$ is the solution of the SCED problem (42)–(46). The resulting $\Delta f(t)$ frequency deviation profile is the subject of interest of this paper.

V. Case Study

The main objective of this paper is to study the impact of wind integration on the power system inertia and its consequent impact on the system frequency deviation from the rated value. This section describes the simulation scenarios necessary to achieve this objective and the simulation setup used in this paper.

It is important to notice, that test systems, in general, are defined by their topology and the generation base. The degree to which these two sets of data is important depends upon how a model depends on these input parameters. As the issues related to the system topology are not central to changes in the system's inertial response, they detract from the central message of the paper regarding the interactions between the SCUC program, the balancing behavior, and the inertial response. It is for this reason, that the paper has specifically focused on the generation base. This paper studies four different scenarios, described in Section V-A, that model different case of wind power integration and the enforcement of inertial response procurement constraints in the SCUC problem.

A. Simulation Scenarios

To allow comparison of the simulation results, four different power system configurations are considered here:

- **Traditional system.** The power system consists of only thermal generation units. The inertia constraints (36)–(37) are ignored.
- **Traditional system with inertia constraints.** Similar to the previous configuration, the power system consists of only thermal generation units. The inertia constraints (36)–(37) are enforced.
- **Wind integrated system.** In addition to the thermal generation units, the system contains wind generation capacity equivalent to 30% of the system peak load. The inertia constraints (36)–(37) are ignored.
- **Wind integrated system with inertia constraints.** Similar to the previous configuration, the system contains wind

generation capacity equivalent to 30% of the system peak load. The inertia constraints (36)–(37) are enforced.

In order to gain insight into the impact of wind integration and the enforcement of inertia constraints, the system behavior of these four configurations are studied within the context of enterprise control assessment. Three behaviors are specifically discussed:

- **Unit commitment.** The unit commitment results for each system configuration are obtained. Integration of the wind alters the number of committed units and consequently the system inertia. Meanwhile, the enforcement of inertia constraints restores the inertia but changes the dispatch levels and their associated costs.
- **Step function response.** The response of the system frequency to a 50MW jump of the load is studied for different combinations of the generation commitment. This serves to understand how different generation commitments alter the dynamics of the system, which eventually defines the system frequency deviation behavior during the operations.
- **Frequency deviation.** The power system operations are simulated for one day period using the enterprise control simulator described above so as to study the system frequency deviations. The results are compared for all four system configurations.

B. Simulation Setup

In order to simulate power system operations, the enterprise control simulator described in Section IV is used. The SCUC formulation in (31)–(41) with inertia procurement constraints is used for commitment of generation units. The real-time dispatch of the committed generators is performed by the SCED formulations in (42)–(46). The physical power grid is represented by the dynamic model of the the IEEE New England test system, consisting of 39 buses and 10 generators [24], where the generators are modeled by the differential equations in Section II-A. Because the New England test system data is originally meant for steady-state power flow analysis, it lacks information about the dynamic properties of the generators. These properties are chosen within reasonable ranges and are aggregated in Table I along with the generation capacities. For simplicity, identical values are assigned to each generator for all the dynamic properties. The daily load and wind profiles are taken from the Bonneville Power Administration (BPA) repositories [25] and the system peak load is 8000MW. This paper also assumes that the wind turbines do not contribute to the inertia of the system. The RoCoF and the frequency nadir limits are taken $0.5Hz/s$ [11], [26] and $0.8Hz$ [9], [11] respectively.

The simulations are performed in the following order. First, the SCUC problem is run to produce the generation commitment schedules for each hour that meet the forecasted demand and maintain the desired RoCoF and frequency nadir. Next, the committed units are dispatched in the real-time balancing operations by the SCED program, and the dispatched values are sent to the dynamic model of the physical power grid as generation setpoints. Finally, the dynamic model of the physical power grid solves the differential equations (47)–(49) to obtain the frequency deviation profiles. The simulations are run for each scenario in Section V-A.

TABLE I
THE PHYSICAL PROPERTIES OF THE GENERATORS

	P^{max} (MW)	P^{min} (MW)	H (s)	D (MW/Hz)	T (s)	R (Hz/MW)	K (MW)
Gen 1	1040	312	15	100	10	0.01	5
Gen 2	646	193.8	15	100	10	0.01	5
Gen 3	725	217.5	15	100	10	0.01	5
Gen 4	652	195.6	15	100	10	0.01	5
Gen 5	508	152.4	15	100	10	0.01	5
Gen 6	687	206.1	15	100	10	0.01	5
Gen 7	580	174	15	100	10	0.01	5
Gen 8	564	169.2	15	100	10	0.01	5
Gen 9	865	259.5	15	100	10	0.01	5
Gen 10	1100	330	15	100	10	0.01	5

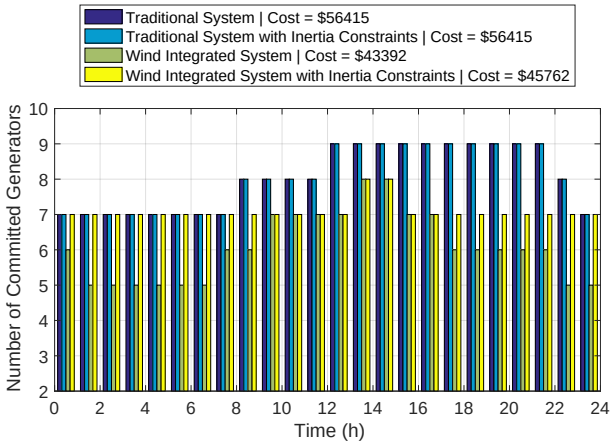

Fig. 3. The number of committed generators for each power system configuration

VI. Results and Discussion

This section reports and discusses the results of the enterprise control simulation. Each of the four power system configurations are simulated and discussed in terms of the three behaviors mentioned above.

A. Unit Commitment

The unit commitment results are obtained for each of four power system configurations. As shown in Table I, although the generators have different capacities and ramping rates, the dynamic characteristics have been set to identical values. Because this paper is focused on the system-wide inertia and dynamic behavior, the relative allocation of inertia to each generator is not of concern. Therefore, the number of committed generators for each operating hour is shown in Fig. 3 as a proxy for the total system-wide inertia.

According to the results in Fig. 3, the commitment of the traditional system is indifferent towards the enforcement of the

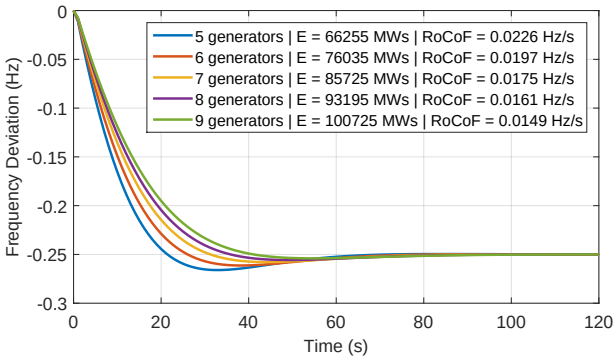

Fig. 4. The response of the system to a loss of 500MW generation unit.

inertia constraints. This is explained by the fact the generation required to meet the daily demand already carries enough inertia to satisfy these constraints. They are not binding. The minimum number of generators is seven. On the other hand, when wind energy is integrated into the power system, the net load drops and the system is able to meet the demand with less generators. During the night, for instance, only five generators is needed to meet the demand. However, when the inertia constraints are enforced, the commitment of the generators changes. Now, there are seven units online during the night. This indicates that the system with only five generators violates the inertia requirement. In this case, the additionally committed units do not generate power. They are online only for maintaining the inertia of the system.

The total operation cost is also affected. As expected, the operation cost drops when wind is integrated into the system as less generation is required to meet the demand. On the other hand, enforcement of the inertia constraints in the presence of wind increases the cost only slightly. This additional cost corresponds to the fixed cost of the generators that don't generate power but are still required to stay online.

B. Inertial Response

Next, the inertial response of the system is simulated for a different number of online generators. This will help to understand how the dynamics of the system change with the reduction of inertia and provide more insight into the results of the frequency deviation presented in the following subsection. As shown in Fig. 3, the number of simultaneously online generators varies from five to nine. Therefore, the inertial response of the system to a 50MW step load increase at $t = 0$ is simulated for 5, 6, 7, 8 and 9 online generation. The corresponding frequency profiles are presented in Fig. 4.

The results in Fig. 4 show that there are two important factors that affect the frequency deviation of the actual system. First, the frequency nadir is lower for the system with less inertia. This shows that for the same load jump, the frequency of the system with lower inertia is more volatile and is more likely to violate the frequency nadir limit. On the other hand, the system with higher inertia has more delay when responding to a load jump. This can also have a negative impact on the ability of the system to fix the frequency deviation after a major jump of the load or a loss of a generator occurs. Thus,

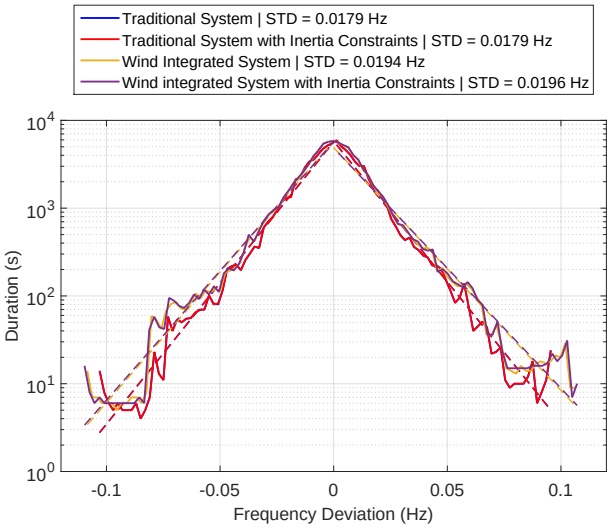

Fig. 5. The distribution of the frequency deviation of different power system configurations

there is no definite answer whether higher inertia is more beneficial for maintaining the system frequency, and it depends on how much role each of these two factors will play. The next subsection studies the impact of these factors on the frequency deviation of the system.

C. Frequency Deviation

As mentioned in the previous section, the frequency deviation depends on how much contribution the differences in frequency nadirs and response delays for the given system inertia will have. To answer that question, the power system operations are simulated for the four configurations described above using the enterprise control simulator. The distributions of the frequency deviations for each configuration are presented in Fig. 5.

Fig. 5 shows the similarity of all four curves relative to each other. As expected, the traditional system has the same frequency deviation for both configurations. The blue curve is hidden behind the red one because they have identical unit commitment as shown above. The distribution for the wind integrated systems is slightly wider, which is not necessarily a result of reduced inertia and can be due to high intermittency of the wind power. The latter is more likely to be true according to Fig. 5 because when the inertia constraints are enforced, the standard deviation increases slightly. However, the impact of inertia on the system frequency is relatively negligible in compared to the impact of the net load intermittency.

Another interesting aspect of Fig. 5 is, that on the logarithmic scale, the trends of the distributions resemble straight lines. Linear least squares regressions are run for each branch of the curves and the results are presented in Fig. 5 by dashed lines. These lines also indicate that while the gap between the traditional and wind integrated system configurations is noticeable, the lines for the configurations with and without inertia constraints are almost indistinguishable.

This work was demonstrated on the IEEE 39-Bus system. The choice of a test case with a relatively small number of

generators demonstrates how small changes in the commitment of generators can have noticeable impacts on the system's RoCoF. Such effects would also appear for much larger systems but only when the penetration of variable energy resources increases accordingly. Because the mathematical model is presented for systems of arbitrary size, the impacts demonstrated here can be expected in other systems of various sizes.

VII. Conclusion

This paper studies the impact of wind integration and enforcement of inertia constraints on the power system frequency deviations. This is achieved by utilizing the two main contributions of this paper. First, generalized expressions for inertial response requirements are derived that keep the system within the given RoCoF and frequency nadir limits. This approach models the dynamics of the system by a second order differential equation, taking the governor with primary control into account. Second, the inertial response requirements are incorporated into the unit commitment problem to study how the presence of these constraints changes the commitment of the generation units for different scenarios of the renewable energy integration. Additionally, different layers of the power system operations are modeled and simulated together so that the generation setpoints from the real-time market are fed into the dynamic model.

The results show that enforcing the inertia constraints has no impact on the unit commitment of the traditional system, while it forces the system to schedule idle generators in the case of the wind integrated system. The results also show that the inertial response is characterized by both its frequency nadir and response delay. A system with greater inertia has a longer settling time and a smaller frequency nadir. Consequently, the distribution of frequency deviations at such small timescales is relatively similar. More importantly, the impact of the system inertia on the frequency deviation is relatively small in comparison to the impact of the net load profile and its intermittency.

References

[1] A. M. Farid, B. Jiang, A. Muzhikyan, and K. Youcef-Toumi, "The need for holistic enterprise control assessment methods for the future electricity grid," *Renewable and Sustainable Energy Reviews*, vol. 56, pp. 669–685, 2016.

[2] A. Muzhikyan, A. M. Farid, and K. Youcef-Toumi, "An Enhanced Method for the Determination of Load Following Reserves," in *American Control Conference 2014 (ACC2014)*, Portland, OR, 2014, pp. 926–933.

[3] A. Muzhikyan, A. M. Farid, and K. Youcef-Toumi, "An Enhanced Method for the Determination of the Ramping Reserves," in *American Control Conference 2015 (ACC2015)*, Chicago, Ill., 2015, pp. 994 – 1001.

[4] A. Muzhikyan, A. M. Farid, and K. Youcef-Toumi, "An Enhanced Method for the Determination of the Regulation Reserves," in *American Control Conference 2015 (ACC2015)*, Chicago, Ill., 2015, pp. 1016 – 1022.

[5] P. Tielens and D. Van Hertem, "The relevance of inertia in power systems," *Renewable and Sustainable Energy Reviews*, vol. 55, pp. 999–1009, mar 2016.

[6] J. F. Restrepo and F. D. Galiana, "Unit commitment with primary frequency regulation constraints," *IEEE Transactions on Power Systems*, vol. 20, no. 4, pp. 1836–1842, 2005.

[7] R. Doherty, G. Lalor, and M. O'Malley, "Frequency Control in Competitive Electricity Market Dispatch," *IEEE Transactions on Power Systems*, vol. 20, no. 3, pp. 1588–1596, 2005.

[8] R. Doherty, G. Lalor, and M. O'Malley, "Correction to "Frequency Control in Competitive Electricity Market Dispatch"," *IEEE Transactions on Power Systems*, vol. 21, no. 2, p. 1015, 2006.

[9] H. Chavez, R. Baldick, and S. Sharma, "Governor Rate-Constrained OPF for Primary Frequency Control Adequacy," *IEEE Transactions on Power Systems*, vol. 29, no. 3, pp. 1473–1480, 2014.

[10] Y. Y. Lee and R. Baldick, "A Frequency-Constrained Stochastic Economic Dispatch Model," *IEEE Transactions on Power Systems*, vol. 28, no. 3, pp. 2301–2312, 2013.

[11] F. Teng, V. Trovato, and G. Strbac, "Stochastic Scheduling With Inertia-Dependent Fast Frequency Response Requirements," *IEEE Transactions on Power Systems*, vol. 31, no. 2, pp. 1557–1566, 2016.

[12] H. Ahmadi and H. Ghasemi, "Security-Constrained Unit Commitment With Linearized System Frequency Limit Constraints," *IEEE Transactions on Power Systems*, vol. 29, no. 4, pp. 1536–1545, 2014.

[13] Y. Wen, W. Li, G. Huang, and X. Liu, "Frequency dynamics constrained unit commitment with battery energy storage," *IEEE Transactions on Power Systems*, vol. 31, no. 6, pp. 5115–5125, 2016.

[14] A. Muzhikyan, A. M. Farid, and K. Youcef-Toumi, "An Enterprise Control Assessment Method for Variable Energy Resource Induced Power System Imbalances. Part I: Methodology," *Industrial Electronics, IEEE Transactions on*, vol. 62, no. 4, pp. 2448–2458, 2015.

[15] A. Muzhikyan, A. M. Farid, and K. Youcef-Toumi, "An Enterprise Control Assessment Method for Variable Energy Resource Induced Power System Imbalances. Part II: Parametric Sensitivity Analysis," *Industrial Electronics, IEEE Transactions on*, vol. 62, no. 4, pp. 2459–2467, 2015.

[16] A. Muzhikyan, A. M. Farid, and K. Youcef-Toumi, "Relative merits of load following reserves & energy storage market integration towards power system imbalances," *International Journal of Electrical Power & Energy Systems*, vol. 74, pp. 222–229, 2016.

[17] B. Jiang, A. Muzhikyan, A. M. Farid, and K. Youcef-Toumi, "Demand Side Management in Power Grid Enterprise Control: A Comparison of Industrial & Social Welfare Approaches," *Applied Energy*, 2017.

[18] A. J. Wood and B. F. Wollenberg, *Power Generation, Operation, and Control*, 3rd ed. New York: J. Wiley & Sons, 2013.

[19] A. Gomez-Exposito, A. J. Conejo, and C. Cañizares, *Electric Energy Systems: Analysis and Operation*. Boca Raton, Fla: CRC Press, 2008.

[20] S. Frank and S. Rebennack, "A Primer on Optimal Power Flow: Theory, Formulation, and Practical Examples," Colorado School of Mines, Tech. Rep. October, 2012.

[21] J. Carpentier, "Contribution to the economic dispatch problem," *Bull. Soc. Franc. Electr.*, vol. 3, no. 8, pp. 431–447, 1962.

[22] B. Stott, J. Jardim, and O. Alsaç, "DC Power Flow Revisited," *Power Systems, IEEE Transactions on*, vol. 24, no. 3, pp. 1290–1300, 2009.

[23] K.-S. Kim, L.-H. Jung, S.-C. Lee, and U.-C. Moon, "Security Constrained Economic Dispatch Using Interior Point Method," in *Power System Technology, 2006. PowerCon 2006. International Conference on*, 2006, pp. 1–6.

[24] R. Zimmerman and C. Murillo-Sanchez, "Matpower 5.1 User's Manual," *Power Systems Engineering Research Center (Pserc)*, pp. 1–116, 2015.

[25] Bonneville Power Administration, "Wind Generation & Total Load in The BPA Balancing Authority." [Online]. Available: http://transmission.bpa.gov/business/operations/wind/

[26] P. Daly, D. Flynn, and N. Cunniffe, "Inertia considerations within unit commitment and economic dispatch for systems with high non-synchronous penetrations," in *PowerTech, 2015 IEEE Eindhoven*, 2015, pp. 1–6.

Aramazd Muzhikyan received his Sc.B and Sc.M degrees from Yerevan State University, Yerevan, Armenia, in 2008. He completed his second Sc.M degree at Masdar Institute of Science and Technology, Abu Dhabi, U.A.E, in 2013. He is currently a PhD student at Thayer School of Engineering at Dartmouth College. His research interests include signal processing, power system optimization, power system operations and renewable energy integration.

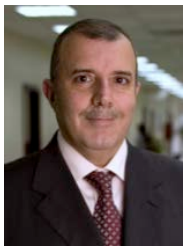

Toufic Mezher is a Professor of Industrial and Systems Engineering at Khalifa University since 2008. He is currently affiliated with the Institute Center for Smart and Sustainable Systems (iSmart). Before Joining Khalifa University, he was a Professor of Engineering Management at the American University in Beirut from 1992 to 2007. He earned a BS in Civil Engineering from University of Florida, and a Master and ScD in Engineering Management from George Washington University in 1988 and 1992 respectively. His research interests include Renewable Energy Management and Policy, Sustainable Development, and Technology Strategy and Innovation Systems.

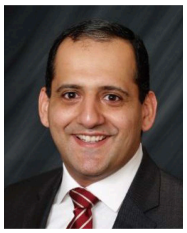

Amro M. Farid received his Sc.B and Sc.M degrees from MIT and went on to complete his Ph.D. degree at the Institute for Manufacturing within the University of Cambridge Engineering Department in 2007. He is currently an associate professor of Engineering and leads the Laboratory for Intelligent Integrated Networks of Engineering Systems (LI^{2}NES) at Thayer School of Engineering, Dartmouth College. He is also a research affiliate at the Massachusetts Institute of Technology – Technology and Development Program. He maintains active contributions in the MIT Future of the Electricity Grid study, the IEEE Control Systems Society, and the MIT-MI initiative on the large-scale penetration of renewable energy and electric vehicles. His research interests generally include the system architecture, dynamics and control of power, water, transportation and manufacturing systems.